Single and multi-resolution extended Kalman ¯lter based reconstruction approaches to optical refraction tomography

Naren Naik,[1] R. M. Vasu,[2] and M. R. Ananthasayanam [3]

[1] *Department of Electrical Engineering*

Indian Institute of Technology, Kanpur

Kanpur- 208016, INDIA.

[2] *Department of Instrumentation*

Indian Institute of Science

Bangalore- 560012, INDIA.

[3] *Department of Aerospace Engineering*

Indian Institute of Science

Bangalore- 560012, INDIA.

Corresponding author: nnaik@iitk.ac.in, nnaikt@yahoo.com

The problem of reconstruction of a refractive-index distribution in optical refraction tomography (ORT) with optical path-length di erence (OPD) data is solved using two adaptive estimation based extended Kalman lter (EKF) approaches. First, a basic single resolution EKF (SR-EKF) is applied to a state variable model describing the tomographic process, to estimate the refractive index distribution of an optically transparent refracting object from noisy OPD data. The initialization of the biases and covariances corresponding to the state and measurement noise is discussed. The state and measurement noise biases and covariances are adaptively estimated. An EKF is then applied to the wavelet transformed state variable model to yield a wavelet based multiresolution EKF (MR-EKF) solution approach.

To numerically validate the adaptive EKF approaches, we evaluate them with benchmark studies of standard stationary cases, where comparative results with commonly used e cient deterministic approaches can can be obtained. Detailed reconstruction studies for the SR-EKF and two versions of the MR-EKF (with respectively Haar and Daubechies-4 wavelets) compare well with those obtained from a typically used variant of the (deterministic) algebraic reconstruction technique, the average correction per projection method, thus establishing the capability of the EKF for ORT. To the best of our knowledge, the present work contains unique reconstruction studies encompassing the use of EKF for ORT in single and multi-resolution formulations, and also in the use of adaptive estimation of the EKF s noise covariances.

OCIS codes: 000.0000, 999.9999.

1. Introduction

1.A. Optical refraction tomography

The optical refraction tomography (ORT) problem arises in various applications such as the optical tomography of the atmosphere, non-invasive evaluation of uid ows, ames, optical bers and other such optically transparent systems. The nonlinear reconstruction problem in ORT [1] is the deducing of the refractive index distribution (RID) of an optically transparent medium, from projection data generated by the propagation of optical waves through the medium under the assumption that di raction e ects are negligible in the propagation process, and only refraction effects exist. Typically, the data used in this class of tomography includes beam-de ections [2], [3], [4], or optical path-length di erences; interferometric [5], [6], [7], [**?**] as well as intensity measurement [9], [10], [11] and wavefront slope measurement based schemes [12], [13]. In our study, the projection data used is the optical path-length di erence (OPD) between the rays propagating through the inhomogeneity to be imaged and the ambient medium.

1.B. Typical solution approaches

Current approaches to the nonlinear reconstruction problem of ORT can be broadly classi ed into (a) deterministic, and (b) stochastic approaches.

The presently used deterministic reconstruction approaches in refraction tomography are mostly iterative techniques to solve the nonlinear system of equations relating the RID to the measured OPD data for all the views under consideration. In various application areas, these iterative techniques are mainly variants of the algebraic reconstruction technique (ART) commonly used in computed tomography, such as the simultaneous algebraic reconstruction technique (SART) [14], or the average correction per projection (ACP) [15] method. In addition, regularized weighted least squares [16], [17] and neural network [18] approaches have been formulated to solve the refraction tomographic problem. Another less used class of methods [19], [20], [21] expresses the actual OPD as the sum of a strictly mathematical quantity, the OPD without refraction (the data that would be obtained in a hypothetical experiment involving the same object, but where refraction has not occurred) and a correction term. The OPD without refraction is then straight path inverted to reconstruct the unknown RID. Time-varying RIDs have been imaged [22], by making OPD measurements for all views simultaneously, and repeating the process at various time instants. The RID at each time instant can then be reconstructed using any of the algorithms mentioned above.

On the other hand, stochastic techniques such as the extended Kalman filter (EKF) have been investigated because of their Bayesian nature as well as their capability to be extended to process time series data. In applications of geophysical travel-time tomography and diffuse optical tomography, Eppstein et.al. [23], [24] have formulated the stationary reconstruction problem in terms of an approximate EKF approach, that uses a suboptimal Kalman update to group zones of similar object-parameter value. On the other hand, for smoothly varying RIDs such as in ORT, Naik et. al. [25], [26], [8] use respectively single and (wavelet based) multiresolution EKF formulations to solve the reconstruction problem of ORT. Kolehmainen et. al. [27] have solved a nonstationary problem in optical diffusion tomography in an EKF setting with a stationary random walk state evolution model. EKFs have also been applied in other tomography settings such as EIT [28] and process tomography [29]. Recently Mukherjee et.al [30] have proposed an EKF to solve a static elastography problem in a dual-grid reconstruction framework.

1.C. Motivation for the present work

In the case of a Kalman filter based reconstruction approach to the linear or nonlinear inverse problems, a major issue is the computational storage and the operations associated with the estimation error covariance matrix that depends upon the size of the state vector being estimated [26]. One way of addressing this issue of compression is to replace the usual state variables (the RID values on the reconstruction grid) by some of their wavelet coefficients via the use of the discrete wavelet transform [31]. In doing so, one reduces the size of the state vector that otherwise had to be estimated in the single resolution case, by using the observation that most of the energy of a smooth signal is contained in its approximate component. We are not aware of any wavelet based EKF approach in tomography other than by Naik and Vasu [26].

A wavelet-transformed Kalman ltering approach (that is inapplicable to computerised tomography though), that attempts to reduce the computational requirements of the lter updates, is suggested by Chin and Mariano [32], [33] for data assimilation tasks in oceanography and meteorology. They derive a Kalman lter approximation, by utilizing an assumption that the correlation between a pair of variables decays exponentially with the distance between the variable locations. A two-dimensional orthonormal discrete wavelet transformation is used to compress the Kalman lter s estimation error covariance matrix (EECM), by transforming it into the so called standard form [34], so as to compute and store only certain elements along certain bands of a given width. The EECM remains in its compressed form in the wavelet transform domain throughout the recursive algorithm. This algorithm is not used for computerised tomography because it uses the spatial locality of the measurements to impose the exponentially decaying correlation structure on the EECM.

Another aspect of Kalman lters is that they are quite sensitive to the measurement and state noise related biases and covariances. Many a time it is not very feasible to have good enough estimates of these covariances. For example, in our work, in order to reduce the computational burden of solving the two-point boundary value problem of ray-linking, we use the centre-out strategy for ray-linking [35], which, due to the data-rebinning strategy it employs to convert the 2-point boundary value problem to an initial value problem, does not lend itself to yielding an apriori estimate of the measurement noise covariance. Further, as is well known, the state noise covariance is a regularizing/stabilizing influence on the reconstructions(by not allowing the EECM to become too small and thereby not neglecting new measurements), and is incorporated into the state variable model even in the absence of any actual state noise [40], [27], [37]. These factors necessitate proper initialization of these parameters, as well as their subsequent adaptive estimation.

Basically, the problem of Kalman filter tuning is to determine the state and measurement noise biases and covariances and the initial EECM, such that the resulting innovations and sample sequences are consistent in their properties with respect to their ensemble (i.e., filter estimated quantities) properties ([36], [37] and references therein). In our work, we have chosen not to augment the state vector with the covariances due to the computational burden, but have estimated it adaptively as the filter processes the measurements as in the seminal work of Myers and Tapley [42].

1.D. Overview of present work

In the present paper, the problem of ORT is solved for the unknown RID in an EKF setting, using adaptive estimation of the necessary process and noise covariances (rather than assumed *apriori* values). We present a detailed study of single and multiresolution EKF reconstruction approaches in ORT. The initialization of the various biases and covariances in the EKF is discussed. To the best of our knowledge, the present work contains the only reconstruction studies using EKF for ORT in single and multi-resolution formulations with the use of adaptive estimation of the EKF s noise covariances.

In the present work, reconstruction studies have been demonstrated for the single resolution EKF (SR-EKF) and two versions of the multi-resolution EKF (MR-EKF) with respectively Haar and Daubechies-4 wavelets. Results of reconstructions using both the EKF based approaches, of two synthetic refractive index distributions from OPD data sets of various noise levels are seen to be comparable with those obtained from a typically used deterministic approach, the average correction per projection method, thus establishing the capability of the EKF for ORT.

The layout of the paper is as follows. The SR-EKF and MR-EKF solutions are described in section 2, with the discrete wavelet transform pre-requisites being the subject of Appendix A. The initialization of the EECM and the state and measurement noise covariances is explained in section 3. Section 4 contains the numerical studies, and section 5 the conclusions of this work. For clarity a list of acronyms is added in Appendix B.

2. Problem de¯nition and EKF reconstruction schemes

2.A. Problem de nition

The reconstruction problem in ORT is to *estimate* the two-dimensional spatial variation of refractive index, $f(x\ y)$ which is embedded in an ambient refractive index, f_{amb}, *given* the noisy optical path-length di erence (OPD) data, $g(\ \ i)$, for view angles $= {}_1 \qquad {}_p$, and rays $i = 1 \qquad m$ (as indexed for each view). The noisy OPD data, $g(\ \ i)$, is expressed as,

$$g(\ \ i) = g^1(\ \ i) + v(\ \ i) \tag{1}$$

with the noiseless OPD $g^1(\ \ i)$ being given by

$$g^1(\ \ i) \qquad {}_{Ray(\ \ i)} f(x\ \ y)ds \quad f_{amb}L \tag{2}$$

where L is the distance between the transmitter and receiver, and, $v(\ \ i)$ is a noise process (frequently assumed Gaussian) representing measurement uncertainties as well as a possible lack of complete satisfaction of the geometrical optics model of light propagation through the RID [15], [6].

The ray paths are obtained by ray-tracing, via integrating the eikonal equation, which is given by

$$\frac{d}{ds}(f\frac{d\mathbf{r}}{ds}) = \quad f \tag{3}$$

where $\mathbf{r}$ is the position vector representing the ray path, and ds is a ray path element. The ray-trace procedure is called a discrete ray-trace or a continuous ray-trace accordingly as the values of the function $f(x\ \ y)$ are known at every point or only at a discrete set of points in space respectively [39].

De ning $\mathbf{f}$ as the row ordered n-vector version of the discrete two-dimensional grid of refractive index values, the reconstruction problem of ORT is to estimate $\mathbf{f}$, *given* $\mathbf{g}(\ {}_i)$=$\mathbf{A}[\mathbf{f}\ \ {}_i]\ \mathbf{f} + \mathbf{v}\ {}_{\mathrm{i}}$, for $i = 1 \qquad p$, where $\mathbf{g}(\ )$ is the OPD vector for view angle ,

$\mathbf{A}[\mathbf{f}]$ is the projection (ray-path) matrix obtained by numerical ray tracing through the discretized RID. Thus, the reconstruction problem of ORT is nonlinear since the ray-path matrix is dependent on the unknown RID (unlike for conventional X-ray CT).

2.B. The EKF approach

A solution scheme to the above defined ORT problem can be a deterministic or a stochastic one. The Kalman filter evaluates the minimum mean square error estimate of a state-vector from noisy observations available for the case of a linear state variable (SV) model governing the dynamical system being studied. The extended Kalman filter [40], [41] is an extension of the linear Kalman filter to the case of a nonlinear SV model governing a physical process, where a Kalman filter is applied to a linear perturbation SV model constructed by linearizing the actual SV model about the most recent estimate of the filter. The aim of setting up an EKF formulation to solve the ORT problem is to develop alternative algorithms to existing approaches, that can ultimately image time-varying RIDs. The present work is limited to time invariant RIDs, the objective being to demonstrate the viability of an EKF algorithm to perform the necessary reconstructions.

2.C. Development of the EKF recursions

The nonlinear continuous-discrete state variable (SV) model for the curved ray tomographic process is given by the following state and measurement equations. The state equation for the view evolution of the RID vector $\mathbf{f}$ can be written as

$$\mathbf{f}(\ \ ) = \mathbf{b}[\mathbf{f}(\ \ )\ \ \mathbf{u}(\ \ )\ \ \ ] + \mathbf{w}(\ \ ) \tag{4}$$

where $\mathbf{u}(\ \ )$ is a state bias vector that is adaptively evaluated in practice and for the static RIDs we are considering in this work, we assume

$$\mathbf{b}[\mathbf{f}(\ \ )\ \ \mathbf{u}(\ \ )\ \ \ ] = \mathbf{0} \tag{5}$$

where, $\mathbf{w}(\ \ )$ is assumed to be a zero-mean continuous white Gaussian noise with covariance $E[\mathbf{w}(\ \ )\mathbf{w}(\ \ )] = \mathbf{Q}(\ \ )\ (\qquad)$. Since $\mathbf{f}$ is modelled as a Gaussian random vector, it is completely speci ed by its mean $\mathbf{f}$ and covariance $\mathbf{P}$ (also called the estimation error covariance matrix (EECM)). The process noise $\mathbf{w}(\ \ )$ and the random initial state $\mathbf{f_0}$, both represent the uncertainty in the actual value of the RID.

The measurement equation describing the relation between the RID and the projection data, for a discrete set of view angles, is

$$\mathbf{g}(\ \ ) = \mathbf{h}[\mathbf{f}(\ \ )\ \ \mathbf{r}(\ \ )\ \ \ ] + \mathbf{v}(\ \ ) \qquad =\ \ _i\ \ i = 1\ \ 2 \tag{6}$$

where $\mathbf{g}(\ \ )$ is the measurement vector corresponding to view angle , $\mathbf{r}(\ \ )$ is a measurement bias term representing the model error due to the uncertainty in the present estimate of the RID, and the measurement function $\mathbf{h}[\qquad]$ is given by

$$\mathbf{h}[\mathbf{f}\ \ \mathbf{r}\ \ \ ] = \mathbf{A}[\mathbf{f}\ \ \ ]\mathbf{f} + \mathbf{r} \tag{7}$$

The measurement noise $(\mathbf{v_i})$ (where $\mathbf{v_i} = \mathbf{v}(\ _i))$ is assumed to be a zero-mean

Gaussian white noise process with covariance $Cov[\mathbf{v}_{\mathbf{i_1}}\ \ \mathbf{v}_{\mathbf{i_2}}] = \mathbf{R}_{\mathbf{i_1}}\ {}_{\mathbf{i_1 i_2}}$. In addition $Cov[\mathbf{v}_{\mathbf{i}}\ \ \mathbf{w}_{\mathbf{i}}]=\mathbf{0}$.

An EKF [40], [41] is now applied to the this state variable model (eqs 4, 6) which re-linearizes the nonlinear system about each new estimate as it becomes available. The EKF recursions for the ORT problem in the predictor-corrector format are given in the box below.

In the notation, $(\mathbf{f_k}, \mathbf{P_k})$ and $(\mathbf{f_k}, \mathbf{P_k}))$ denote the ltered and predicted estimates respectively obtained after processing measurement $\mathbf{g_k}$. The *a priori* unknown biases and covariances in the EKF recursions, $\mathbf{Q_k}\ \mathbf{r_k}\ \mathbf{R_k}$ are adaptively evaluated in our present work as the lter processes the measurements by the covariance-estimating technique proposed by Myers and Tapley [42], which computes the desired covariances by comparing a calculated estimate with that obtained from the relevant samples of the biases, using a sliding window of considered measurements. We note that while in general we can consider a non-zero state bias $\mathbf{u}$ that needs to be adaptively estimated, the xing of the state bias all through the EKF recursions has been justi ed by the observation that both the state and measurement biases cannot be simultaneously estimated by the Myers and Tapley estimator because of the proportioning of any one of the biases into the two estimators for the state and measurement covariances [43]. The speci c choice of zero state bias in our work has been justi ed by several simulation runs as well.

I *Initialization:* Set $\mathbf{f_0}$, $\mathbf{P_0}$, $\mathbf{Q_0}$, $\mathbf{r_0}$, $\mathbf{R_0}$ as explained in Section 3.

For $k = 1\ 2$, till convergence

II *Prediction equations*

$\mathbf{f_{k+1}} = \mathbf{f_k}$

$\mathbf{P_{k+1}} = \mathbf{P_k} + \mathbf{Q_k}$

III *Measurement bias and covariance estimation (k L_r)*

(a). Bias sample, $\mathbf{r_k}$ $\mathbf{g_k}$ $\mathbf{A_k f_k}$ where $\mathbf{A_k}$ $\mathbf{A}[\mathbf{f_k}\ \mathbf{k}]$; Covariance sample $_{\mathbf{k}}$ $\mathbf{A_k P_k A_k}$.

(b). De ning $(p\ q)$ $(\mathbf{r_p}$ $\mathbf{r_q})(\mathbf{r_p}$ $\mathbf{r_q})^T$, $^{\mathbf{1}}(p\ q)$ $(\mathbf{r_p}$ $\mathbf{r_q})(\mathbf{r_p}$ $\mathbf{r_q})^T$,

$\mathbf{r_k} = \mathbf{r_{k\ 1}} + \frac{1}{L_r}(\mathbf{r_k}$ $\mathbf{r_{k\ L_r}})$

$\mathbf{R_k} = \mathbf{R_{k\ 1}} + \frac{1}{L_r\ 1}$ $(k\ k)$ $(k$ $L_r\ k) + \frac{1}{L_r}$ $^{\mathbf{1}}(k\ k$ $L_r) + \frac{L_r\ 1}{L_r}($ $_{\mathbf{k\ L_r}}$ $_{\mathbf{k}})$

(c). Shift noise samples : $\mathbf{r_j} = \mathbf{r_{j+1}}$, $_{\mathbf{j}} =$ $_{\mathbf{j+1}}$, $j = k$ L_r k 1

IV *Kalman Gain*

$\mathbf{K_{k+1}} = \mathbf{P_k A_k^T}[$ $_{\mathbf{k}} + \mathbf{R_k}]$ ^{1}

V *Correction equations (State estimation)*

$\mathbf{f_k} = \mathbf{f_k} + \mathbf{K_k}(\mathbf{r_k}$ $\mathbf{r_k})$

$\mathbf{P_k} = (\mathbf{I}$ $\mathbf{K_k A_k})\mathbf{P_k}$

VI *State noise estimation*

(a). $_k = \mathbf{P_{k\ 1}}$ $\mathbf{P_k}$

(b). $\mathbf{Q_k} = \mathbf{Q_{k\ 1}} + \frac{1}{L_q}$ $_{\mathbf{k\ L_q}}$ $_{\mathbf{k}}$

(c). Shift noise samples: $_{\mathbf{j}} =$ $_{\mathbf{j+1}}$, $j = k$ L_q k 1

2.D. The waveletized EKF

In the case of a Kalman filter based reconstruction approaches to the linear or non-linear inverse problems, a major issue, is the computational effort with respect to storage and the number of floating point operations associated with the estimation error covariance matrix (EECM), **P**, which in turn depends upon the size of the state vector being estimated.

Wavelet based solution approaches, in essence, solve the wavelet transformed versions of the reconstruction problem, and are fundamentally motivated by the generic property of the wavelet transform that yields a multiresolution decomposition of a signal into its coarse and fine components in space. The wavelet transform of the measurement operator sparsifies it by focussing the useful information on a small number of entries, other coefficients being small enough to be neglected by an appropriate choice of a threshold [44], [45]. Further one can motivate waveletizing the respective inverse problems by noting that the expansion of **f** in a wavelet basis provides a natural mechanism for adapting the level of detail in the reconstruction to the information content in the data, thereby stabilizing the solution procedure, i.e. one can decide the regions of the reconstructions where only the coarse scale estimates are needed and those where one needs the added detail [38], [46]. Also, orthonormal wavelets are bases for function spaces containing edgy objects and can be used as edge preserving regularisers [38], [47].

In our work, an EKF is applied to the wavelet transformed state variable model describing the tomographic process, in order to solve the reconstruction problem of ORT. Denoting the $2D$ DWT matrix for wavelet transforming $\mathbf{f}$ by $\mathbf{W}_2$ (see appendix for details), the wavelet transformed state equation is obtained as

$$\mathbf{f}(\ ) = \mathbf{w}(\ ) \tag{8}$$

where $\mathbf{z} = \mathbf{W}_2\mathbf{z}$ for any two-dimensional concatenated vector $\mathbf{z}$, $\mathbf{w_k}(\ )$ is the wavelet transformed continuous noise process with zero mean and covariance $E[\mathbf{w}(\ )\mathbf{w}(\ )] =$ $\mathbf{Q}(\ )\ (\qquad)$, where $\mathbf{Q} = \mathbf{W}_2\mathbf{Q}\mathbf{W}_2$.

Denoting the one-dimensional DWT matrix for wavelet transforming a data vector by $\mathbf{W}_1$, the wavelet transformed measurement equation is obtained from eqn(6) as

$$\mathbf{g}(\ ) = \mathbf{h}[\mathbf{f}(\ )\ \mathbf{r}(\ )\quad] + \mathbf{v}(\ ) \qquad = \ _i\ i = 1\ 2 \tag{9}$$

where $\mathbf{h}[\qquad]$ is given by

$$\mathbf{h}[\mathbf{f}\ \mathbf{r}\quad] = \mathbf{A}[\mathbf{f}\quad]\mathbf{f} + \mathbf{r} \tag{10}$$

where $\mathbf{A} = \mathbf{W}_1\mathbf{A}\mathbf{W}_2$, and the measurement noise $(\mathbf{v_i})$ (where $\mathbf{v_i} = \mathbf{v}(\ _i)$) is a zero-mean Gaussian white noise process with covariance $Cov[\mathbf{v_{i_1}}\ \mathbf{v_{i_2}}] = \mathbf{R_{i_1}}\ _{\mathbf{i_1 i_2}}$, where $\mathbf{R} = \mathbf{W}_1\mathbf{R}\mathbf{W}_1$.

The assumption of uncorrelated noise processes $\mathbf{v_k}$, and $\mathbf{w}(\ )$, each being uncorrelated between views in the original state variable model results in respective, view-uncorrelated noise processes in the wavelet domain too because of the orthonormality of the DWT matrices.

In our present work, however we use $\mathbf{W}_1 = \mathbf{I}$, so that the measurements are not actually wavelet transformed despite the state vector being so. This has been done since the results of several simulational runs showed that better results were consistently obtained by the above choice of $\mathbf{W}_1$, rather than setting it to be a DWT matrix.

An EKF is now applied to the above wavelet transformed state variable model to estimate only the approximate component of the state vector. This is justified because of the property that most of the energy in the original RID(assumed to be a smooth function in ORT applications) is contained in the approximate sub-image of its wavelet transform. In addition, the above restriction reduces the dimension of the state vector that has to be estimated, over that in the single resolution case, thus reducing the computational requirements of the estimation process.

The EKF recursion equations are thus of the same form as in the SR-EKF (in box at end of previous subsection), with all quantities being replaced by their appropriately wavelet transformed quantities. We neglect the contribution from the detail part of the DWT of $\mathbf{P}$, considering that the possibility of spurious detail related error covariances adversely affecting the estimate of $\mathbf{f}$, is greater than the possibility of the detail component of the DWT of $\mathbf{f}$ being significantly different from its first estimate, for the smooth RIDs being reconstructed in ORT. Thus, $\mathbf{A_k}[\mathbf{f_k}\ k]$ is the approximate component of the wavelet transform of the ray-path matrix.

3. Initialization

The initial estimate of the RID, $\mathbf{f_0}$ is obtained by inverting the noisy OPD data assuming no refraction has occurred, by using the convolution backprojection algorithm commonly used in straight path X-ray tomography, and by subsequent smoothing of the straight path estimate.

Initialization of the above mentioned biases and covariances is done by semi-heuristic means outlined below. The initialization of the covariances requires the stipulation of the *a priori* EECM, $\mathbf{P_0}$. In our study, $\mathbf{P_0}$ has been formed on the basis of the starting estimate of the RID, $\mathbf{f_0}$. An initial RID estimate is also needed for the evaluation of the initial ray-path matrices at the first iteration, which in turn, along with the knowledge of $\mathbf{P_0}$, are instrumental in yielding the desired initialization of the model error, $\mathbf{r_0}$, and noise covariance, $\mathbf{R_0}$. We now briefly describe the initialization of the various parameters.

3.A. Stipulation of $\mathbf{P_0}$

In practice, in both linear and nonlinear estimation problems, the choice of $\mathbf{P_0}$ has a strong bearing on the behaviour of the Kalman filter, especially considering that in general we do not have good knowledge of the state and measurement biases and covariances. In our study, we have used a heuristic procedure to estimate $\mathbf{P_0}$, the choice of procedure being verified by several trial simulational runs. The two-step procedure is as follows:

Step 1. For every view of the ctitious centre-out ray tracing strategy, obtain the OPD and the corresponding ray-path matrix by discrete ray-tracing through the starting estimate of the RID, $\mathbf{f_0}$, and thus form the concatenated measurement vector as $\mathbf{g}$ and the corresponding ray-path matrix as $\mathbf{A}[\mathbf{f_0}]$. Then evaluate the di erence vector $(\mathbf{g} \quad \mathbf{A}[\mathbf{f_0}]\mathbf{f_0})$.

Step 2. Assuming $\mathbf{g} \quad \mathbf{A}[\mathbf{f_0}]\mathbf{f}$, where $\mathbf{f}$ is the actual unknown RID, we evaluate a rough estimate of $\quad \mathbf{f_0} = (\mathbf{f} \quad \mathbf{f_0})$ by straight-path inversion of the vector $(\mathbf{g} \quad \mathbf{A}[\mathbf{f_0}]\mathbf{f_0})$.

Now stipulate $\mathbf{P_0}$ to be a diagonal matrix, with entries $\mathbf{P_0}(i \ \ i) = (\quad \mathbf{f}(i))^2$.

We have observed through numerical sensitivity studies around this choice of $\mathbf{P_0}$ (with $\mathbf{Q}$ and $\mathbf{R}$ being adaptively estimated) that the reconstructions have been found to not change much for modest variation, but for large variation the results do deteriorate enormously similar to the feature noticed by Sarkar [37].

3.B. Stipulation of $\mathbf{Q_0}$*,* $\mathbf{r_0}$ *and* $\mathbf{R_0}$

We set the initial state noise covariance, $\mathbf{Q_0}$ as being the zero matrix. Recall from the previous section that the state bias is retained at the zero vector all through the recursions.

The evaluation of the initial measurement noise covariance, $\mathbf{R_0}$, is presented below. A covariance estimating approach similar in spirit to the Myers and Tapley procedure has been used, with the initial measurement bias, $\mathbf{r_0}$ being evaluated enroute.

An intuitive sample of the sum of the model error bias and the zero mean measurement noise is

$$\mathbf{r}_{\mathbf{j}}^{\mathbf{s}} = \mathbf{g}_{\mathbf{j}} \quad \mathbf{A}_{\mathbf{j}}\mathbf{f}_{\mathbf{0}} \tag{11}$$

where here $\mathbf{A}_{\mathbf{j}} = \mathbf{A}[\mathbf{f}_{\mathbf{0}} \ \mathbf{j}]$.

Thus, the covariance as predicted by the lter statistics is

$$Cov(\mathbf{r}_{\mathbf{j}}^{\mathbf{s}}) = \mathbf{A}_{\mathbf{j}}\mathbf{P}_{\mathbf{0}}\mathbf{A}_{\mathbf{j}} + \mathbf{R}_{\mathbf{j}} \tag{12}$$

where we have assumed $\mathbf{g}_{\mathbf{j}} \quad \mathbf{A}_{\mathbf{j}}\mathbf{f}$, $\mathbf{f}$ being the actual unknown RID.

Considering the calculated covariance in turn as a random variable, the predicted (by lter statistics) estimate of $Cov(\mathbf{r}_{\mathbf{j}}^{\mathbf{s}})$ over the calculation window is given by the sample mean of the individual calculated covariances, and is obtained as

$$\mathbf{C}_{\mathbf{r}}^{\mathbf{pred}} = \frac{{}_{j=1}^{j=L_r} \quad {}_{\mathbf{j}}}{L_r} + \mathbf{R}_{\mathbf{0}} \tag{13}$$

where L_r is the length of a calculation window, and,

$$_{\mathbf{j}} = \mathbf{A}_{\mathbf{j}}\mathbf{P}_{\mathbf{0}}\mathbf{A}_{\mathbf{j}} \ \ \mathbf{R}_{\mathbf{0}} = \frac{{}_{j=1}^{j=L_r} \mathbf{R}_{\mathbf{j}}}{L_r} \tag{14}$$

Assuming ergodicity, the unbiased estimate of the covariance as obtained from the sample over the calculation window can also be found from the relation,

$$\mathbf{C}_{\mathbf{r}}^{\mathbf{derived}} = \frac{{}_{j=1}^{j=L_r} (\mathbf{r}_{\mathbf{j}}^{\mathbf{s}} \quad \mathbf{r}_{\mathbf{0}})(\mathbf{r}_{\mathbf{j}}^{\mathbf{s}} \quad \mathbf{r}_{\mathbf{0}})}{L_r \quad 1} \tag{15}$$

where $\mathbf{r}_{\mathbf{0}}$ is an estimate of the mean of the random process represented by the noise samples, and is usually computed as the sample mean given by

$$\mathbf{r}_{\mathbf{0}} = \frac{{}_{j=1}^{j=L_r} \mathbf{r}_{\mathbf{j}}}{L_r} \tag{16}$$

The quantity $\mathbf{r_0}$ is a measure of the initial measurement bias because of the zero mean assumption on the measurement noise process.

Hence the initial noise covariance $\mathbf{R_k}$ is obtained by comparison of the expressions for $\mathbf{C_r^{pred}}$ and $\mathbf{C_r^{derived}}$ as

$$\mathbf{R_0} = \mathbf{C_r^{meas}} \quad \frac{{}_{j=1}^{j=L_r} \quad \mathbf{j}}{L_r} \tag{17}$$

In practice, if any of the entries of the covariance matrix are negative, then we replace it with its absolute value as suggested in [42].

4. Numerical studies

In order to numerically validate the above presented EKF based algorithms, they are applied to the reconstruction of mildly refracting RID phantoms.

4.A. Test cases

In the present work, we have considered two mildly refracting phantoms, a double Gaussian phantom [5], as shown in Fig.1a, and, an axisymmetric Gaussian RID as shown in Fig.1b. The double Gaussian RID denoted as phantom $P1$, which might be representative of the RID in a cross-section of the plume above an unevenly heated object submerged in water, is given by

$$f(x \;\; y) = f_{amb} \quad 0\;01 f_{amb}[exp(\quad \frac{x^2 + (y \quad 0\;1)^2}{0\;09}) + exp(\quad \frac{x^2 + (y + 0\;5)^2}{0\;04})] \tag{18}$$

The axisymmetric single Gaussian phantom, denoted by $P2$, has the functional

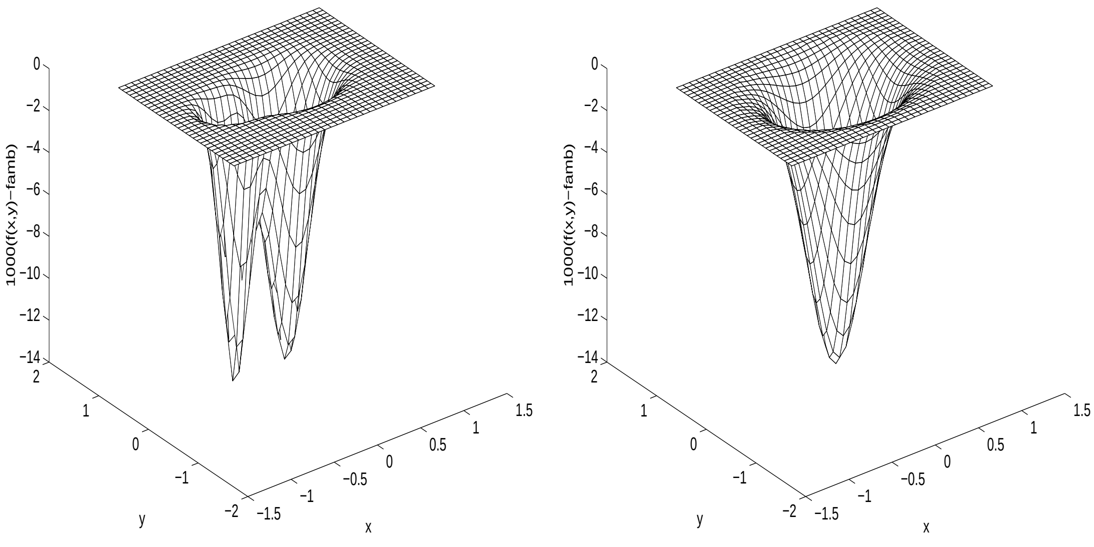

(a) (b)

Fig. 1. (a) Surface mesh pro le of phantom $P1$ (b) Surface mesh pro le of phantom $P2$

form

$$f(x\ \ y) = f_{amb} \quad 0\ 01 f_{amb} exp(\quad \frac{x^2 + y^2}{0\ 18}) \tag{19}$$

where, following [5], $f_{amb} = 1\ 3321$.

Noiseless, OPD data is simulated for 16 views and 40 rays per view by continuous ray-tracing through each of the above RIDs. Subsequently zero mean independent Gaussian random noise of variances $\ ^2 = 0\ 16$ and $\ ^2 = 0\ 25$ are added to the noiseless OPD data of the rst double Gaussian phantom in turns, to generate two slightly overdetermined data sets denoted as $P1D1$ and $P1D2$, with signal to noise ratios $21\ 300dB$ and $19\ 4063dB$ respectively. Zero mean independent Gaussian random noise of variances $\ ^2 = 0\ 25$ and $\ ^2 = 0\ 36$ are added to the noiseless OPD data of the second axisymmetric Gaussian phantom in turns,to generate two data sets corresponding to the second phantom, denoted as $P2D1$ and $P2D2$, with signal to noise ratios 21 05066dB and 19 17865dB respectively.

4.B. Simulational details and results

The error measure used in our simulations is the average error defined by

$$error_{av} = \sum_{i=1}^{n} \frac{\left|\, \hat{\mathbf{f}}(i) - \mathbf{f}(i) \,\right|}{N f_{min}} \tag{20}$$

where N is the dimension of the state vector, and f_{min} is the absolute value of the minimum value of the actual RID.

The starting estimate of the RID is obtained by straight path inversion of the projection data using the filtered backprojection algorithm [48], followed by smoothing. The size of the two-dimensional RID reconstruction grid considered is 32×32. In addition, the discrete ray tracing scheme(to generate the projection matrix for a nominal value of the RID obtained after processing the OPD data corresponding to a view) in this work follows the centre-out strategy for ray-linking [35].

The EKF algorithm used in our present study, makes use of, without any loss of generality, a simplification [40] in the update procedure for the case of a diagonal noise covariance matrix, **R**, with the update recursion equations being modified as mentioned in the introduction of the thesis. The EKF prediction and update recursions are carried out using the U-D factorisation technique [49], to reduce the susceptibility of the EKF to roundoff errors and numeric instability.

In the study presented in this paper, we have implemented the MR-EKF for single-level wavelet transformations only, using the Haar and the Daubechies-4 (Db-4) wavelets to perform the DWT operations. The filter coefficients of two wavelets used in this work are as below :

The Haar wavelet has the coefficients :

$$h_0 = h_1 = \frac{1}{\sqrt{2}} \qquad g_k = (-1)^k h_{1-k} \; k = 0, 1 \tag{21}$$

The Daubechies-4 wavelet has the coefficients :

$$h_0 = \frac{1+\sqrt{3}}{\sqrt{2}} \; h_1 = \frac{3+\sqrt{3}}{\sqrt{2}} \; h_2 = \frac{3-\sqrt{3}}{\sqrt{2}} \; h_3 = \frac{1-\sqrt{3}}{\sqrt{2}} \qquad g_k = (-1)^k h_{1-k} \; k = 0, 1, 2, 3 \tag{22}$$

In the evaluation of the appropriate wavelet transform of the ray-path matrix we have utilized the scheme suggested by Zhu etal [46]. First, each row is reordered into an $N_x \times N_y$ matrix (where the image we are reconstructing is assumed to be $N_x \times N_y$), to which the separable transform, $\mathbf{W}_2$ is applied. After this separable transformation, we reorder the transformed matrix back into a row, as before, to obtain an intermediate matrix that we denote by $\mathbf{A}^{\mathbf{row}}$. Then each column of this matrix, we operate $\mathbf{W}_1$, to obtain the transformed projection matrix, $\mathbf{A}$.

The *a priori* constraints used are those relating to the value bounds and support of the RID. For the axisymmetric phantom, $P2$, we do not utilize its axisymmetry as an *a priori* constraint. In the present studies, it has been observed after many simulational runs that reasonable convergence to the actual estimate is invariably obtained in a couple of iterations itself. The convergence criteria used in our study is a combination of the average error estimated and visual perception of features of interest. Owing to the dependence of the ray path matrix on the computed estimate, the algorithms, after achieving a "best" estimate, tend to diverge away from that value due to effects of finite precision and roundoff errors. This phenomenon of divergence has been observed in this class of problems in past studies too [5], [15], and recourse to stopping the reconstruction process after a fixed number of iterations has also been suggested in other works [50]. In our work, after the application of the object support constraint, we have $N = 553$ for the SR-EKF, $n = 152$ for the Haar wavelet based EKF, and $n = 181$ for the Db-4 wavelet based EKF.

Figures 2-9 give the surface mesh plots and cross-sectional reconstructions for the two phantoms, obtained after two iterations (an iteration being one complete pass through the projection data) from the SR-EKF, MR-EKF and ACP algorithms, for various noise levels of the projection data. The quantity plotted in all the figures is $1000(f(x,y) - f_{amb})$. The cross-sectional figures plot the RID estimate through the plane $x = 0$, i.e, $1000(f(x = 0, y) - f_{amb})$. We observe that across the test cases considered, the EKF based algorithms achieve comparable performance to the ACP, both with respect to the error estimates and visual perception. As expected in the MR-EKF, we observe that the (smoother) Db-4 wavelet based MR-EKF does better than the Haar EKF. The observation that the cross sectional images of the SR-EKF in general track the features of interest better than the MR-EKF indicates that the use of the detail components in certain regions of the reconstruction needs to be considered for more accurate reconstruction. The average errors obtained after two iterations for the multiresolution and single resolution EKF, and ACP algorithms are tabulated below.

Data set	Haar MR-EKF	Db-4 MR-EKF	SR-EKF	ACP
$P1D1$	2 3525%	1 8052%	1 7982%	1 8354%
$P1D2$	2 3991%	2 1118%	2 1536%	2 2157%
$P2D1$	3 1236%	3 0939%	2 6084%	2 4784%
$P2D2$	3 4932%	3 2353%	3 2012%	2 9946%

The comparability of EKF and ACP results are signi cant since the ACP approach (and its SART or SIRT type cousins) are among the most e cient algorithms for static RIDs. These benchmarking studies thus give the necessary pre-requisite insight necessary for the use of the EKF in ORT for cases where the RIDs may be varying in time.

5. Conclusions and further directions

The problem of refractive-index reconstruction in ORT with optical path-length difference (OPD) data is solved using two adaptive estimation based EKF approaches. A single resolution EKF (SR-EKF) is applied to a state variable model describing the tomographic process, to estimate the RID of an optically transparent refracting object from noisy OPD data. The state and measurement noise biases and covariances

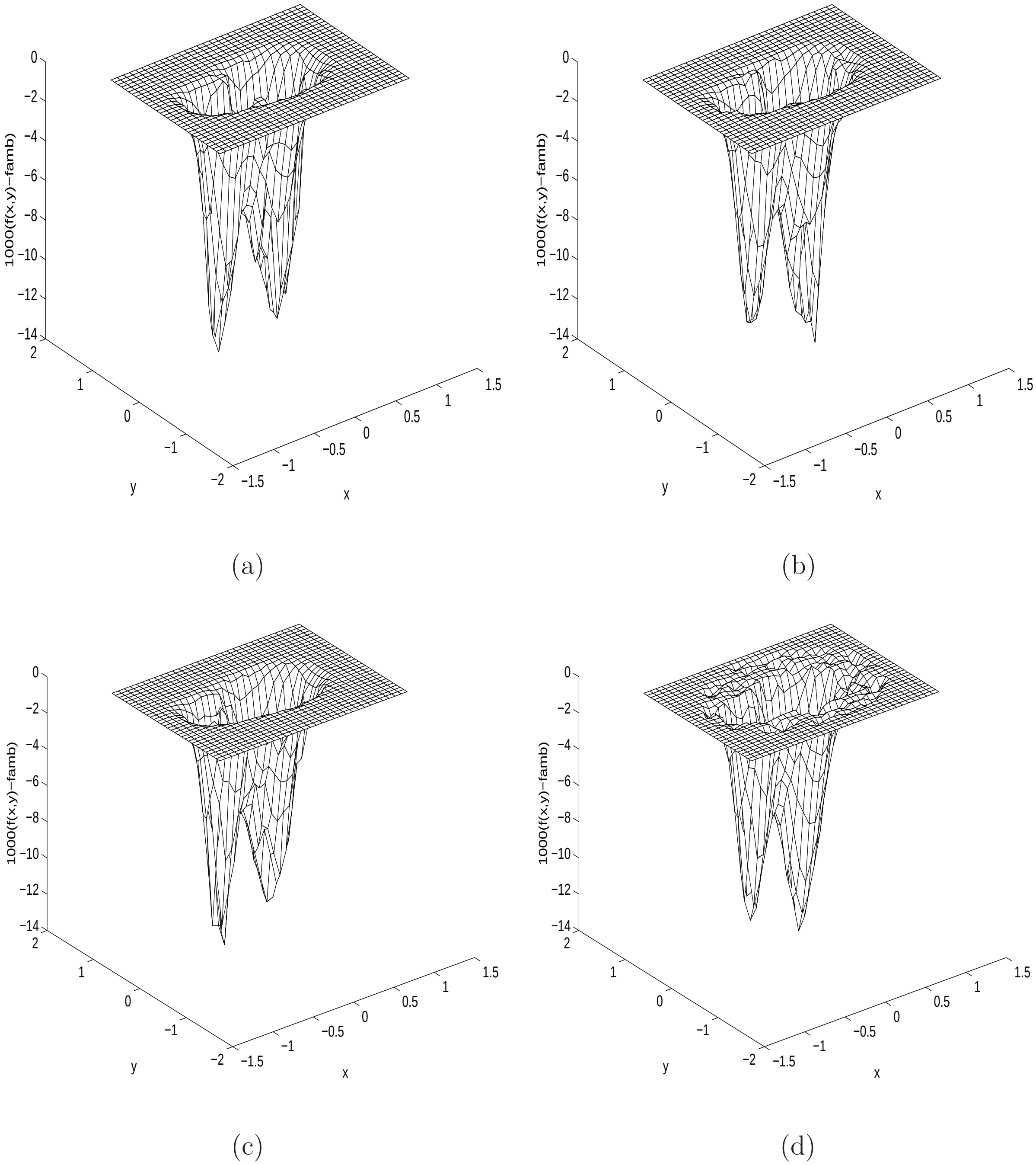

Fig. 2. Reconstructed surface mesh pro les of the phantom $P1$ obtained for the data set $P1D1$ after the second iteration by (a) the Haar MR-EKF, (b) the Db-4 MR-EKF, (c) the SR-EKF, and, (d) the ACP algorithm.

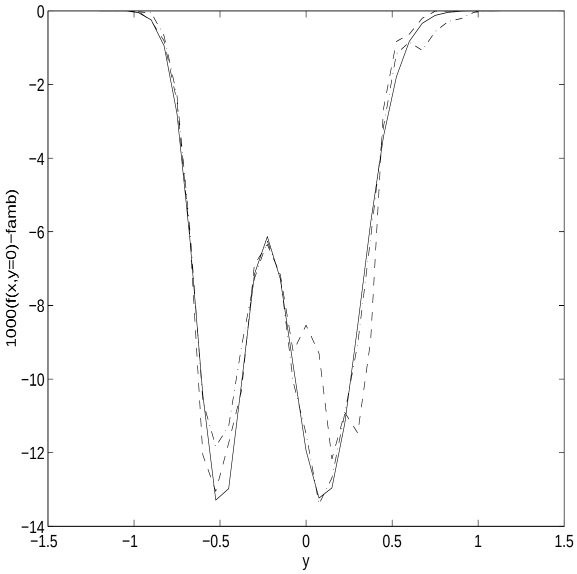

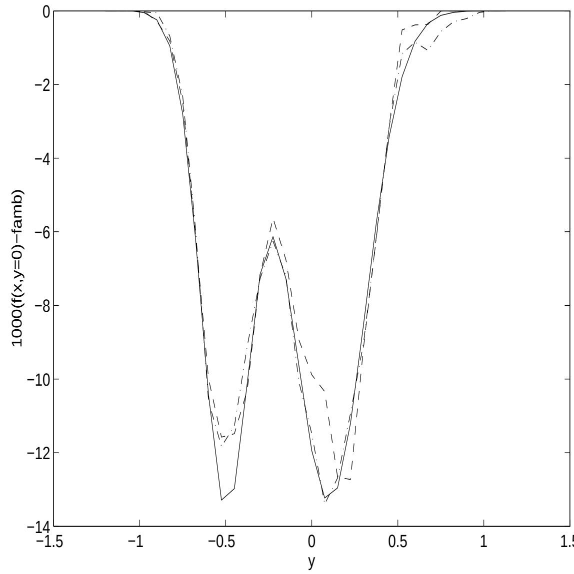

(a) (b)

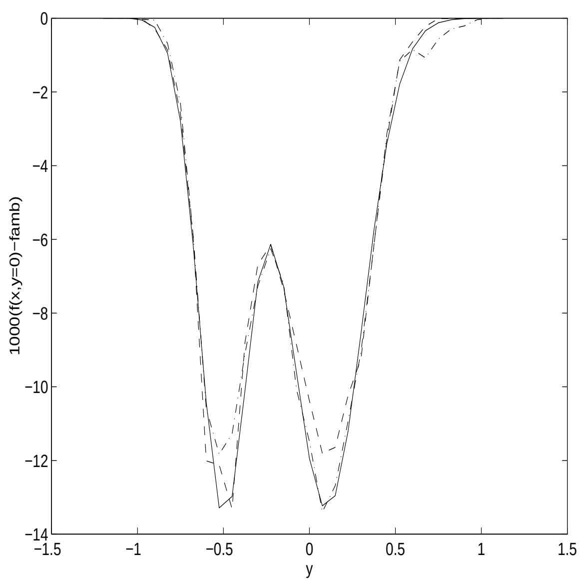

(c)

Fig. 3. Reconstructed pro les of the $x = 0$ plane of phantom $P1$ obtained from the EKFs(dashed curves), as compared to ACP (dot-dash curve) algorithm and the actual pro le (solid line) for the data set $P1D1$ after the second iteration by (a) the Haar MR-EKF, (b) the Db-4 MR-EKF, and, (c) the SR-EKF algorithm.

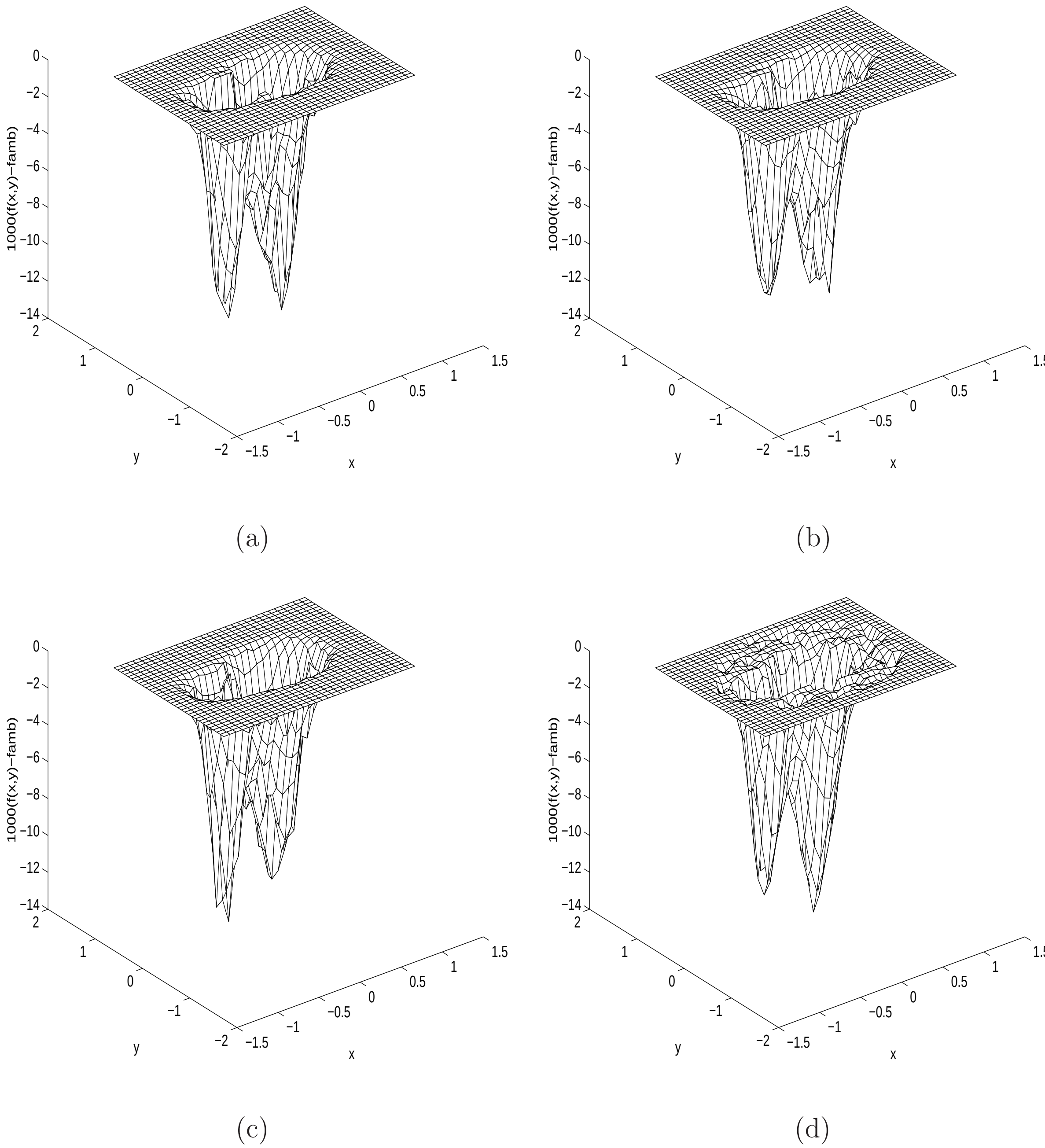

Fig. 4. Reconstructed surface mesh pro les of the phantom $P1$ obtained for the data set $P1D2$ after the second iteration by (a) the Haar MR-EKF, (b) the Db-4 MR-EKF, (c) the SR-EKF, and, (d) the ACP algorithm.

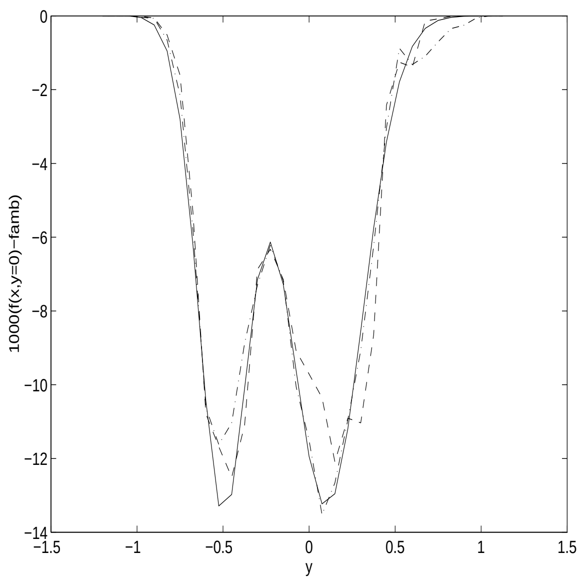

(a)

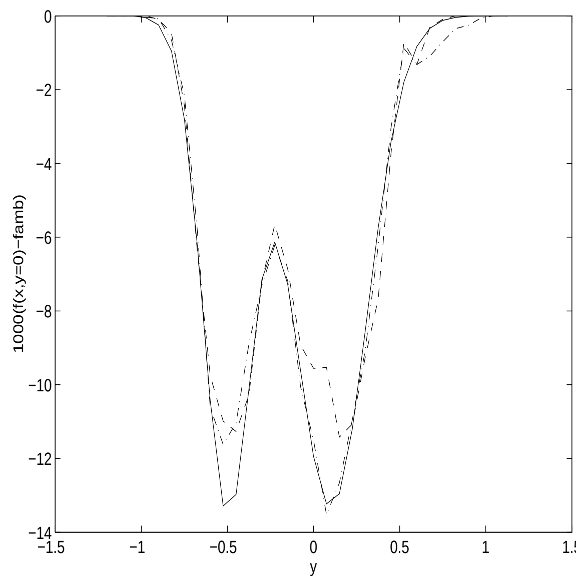

(b)

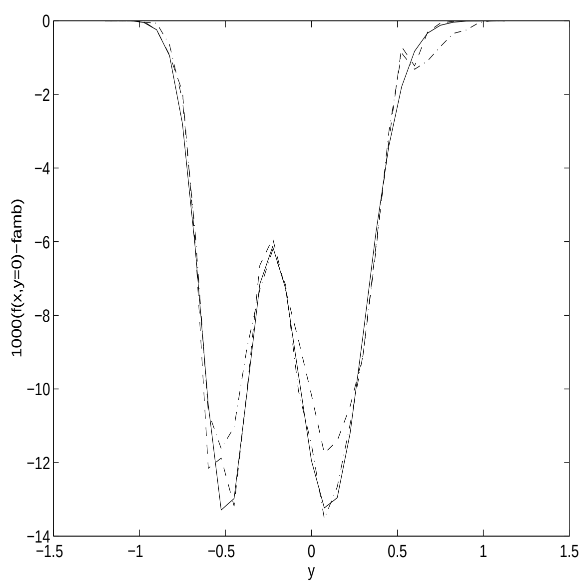

(c)

Fig. 5. Reconstructed pro les of the $x = 0$ plane of phantom $P1$ obtained from the EKFs(dashed curves), as compared to ACP (dot-dash curve) algorithm and the actual pro le (solid line) for the data set $P1D2$ after the second iteration by (a) the Haar MR-EKF, (b) the Db-4 MR-EKF, and, (c) the SR-EKF algorithm.

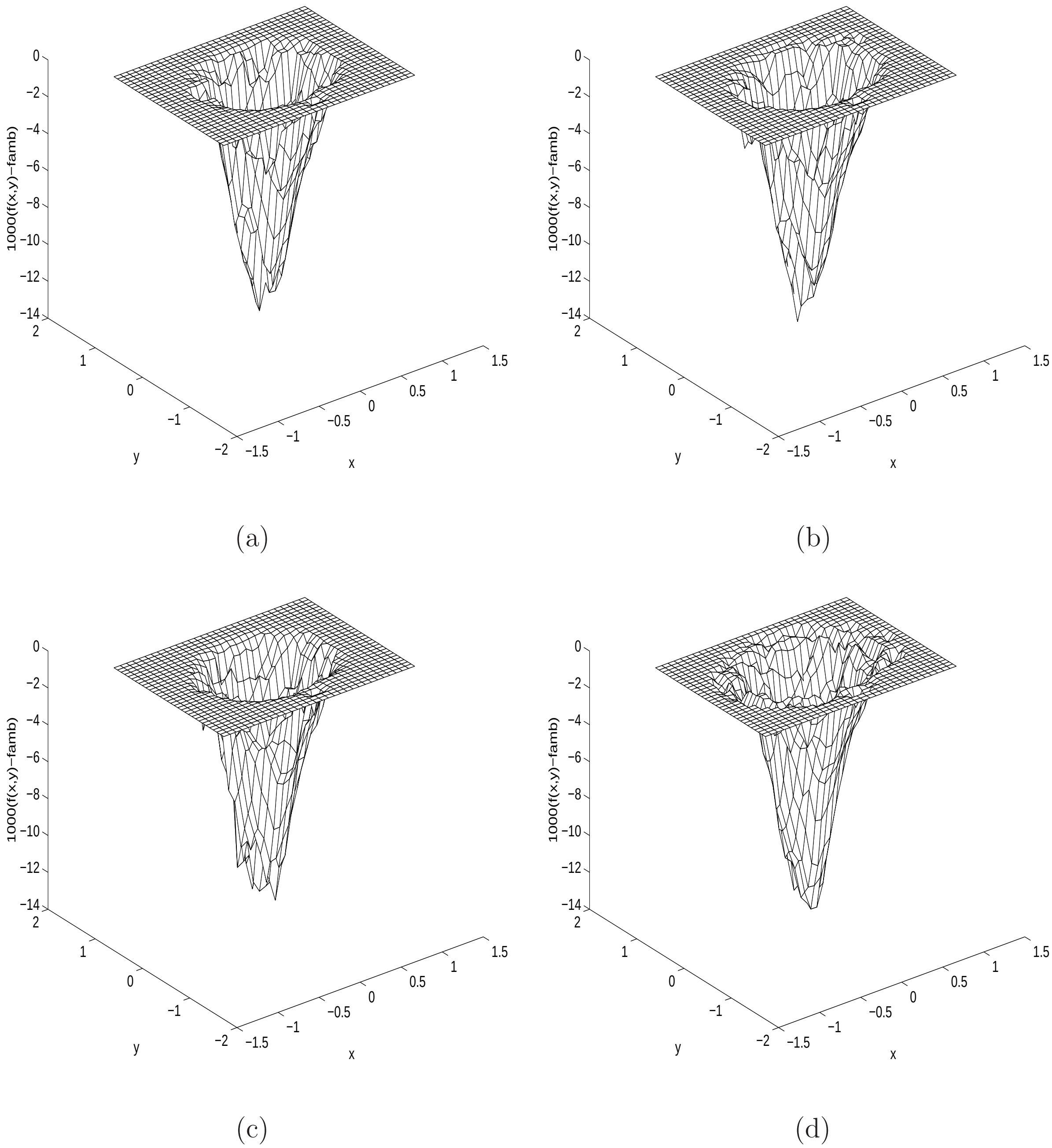

Fig. 6. Reconstructed surface mesh pro les of the phantom $P2$ obtained for the data set $P2D1$ after the second iteration by (a) the Haar MR-EKF, (b) the Db-4 MR-EKF, (c) the SR-EKF, and, (d) the ACP algorithm.

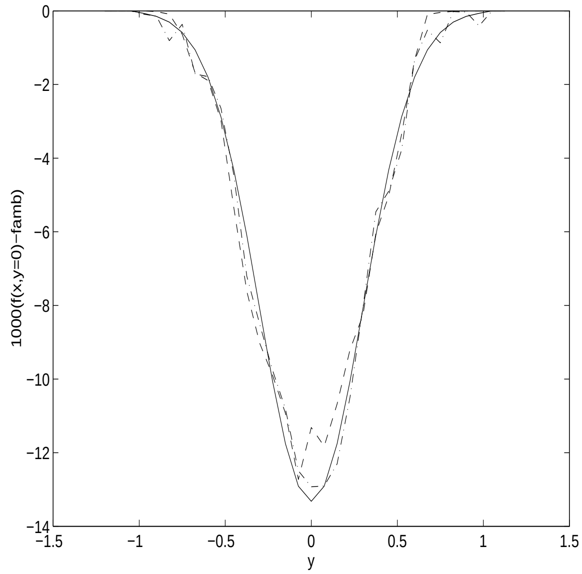

(a)

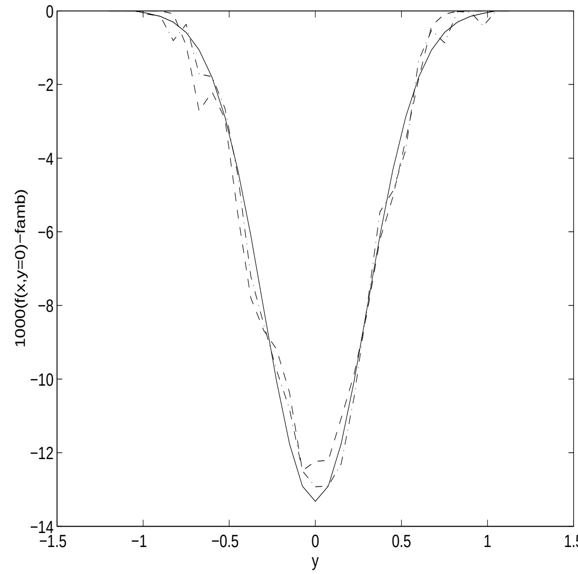

(b)

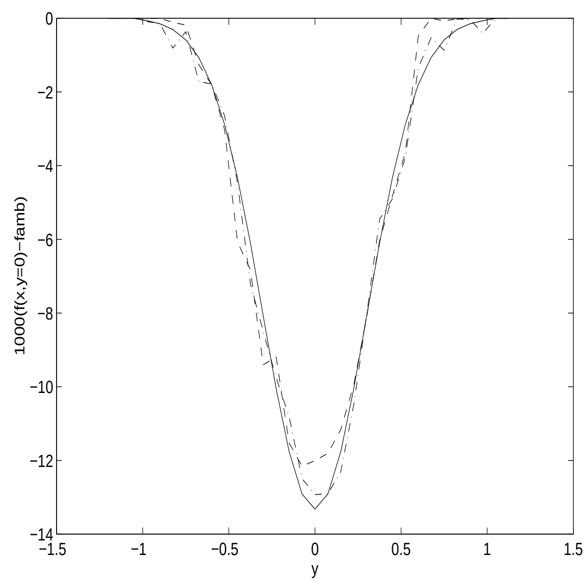

(c)

Fig. 7. Reconstructed pro les of the $x = 0$ plane of phantom $P2$ obtained from the EKFs(dashed curves), as compared to ACP (dot-dash curve) algorithm and the actual pro le (solid line) for the data set $P2D1$ after the second iteration by (a) the Haar MR-EKF, (b) the Db-4 MR-EKF, and, (c) the SR-EKF algorithm.

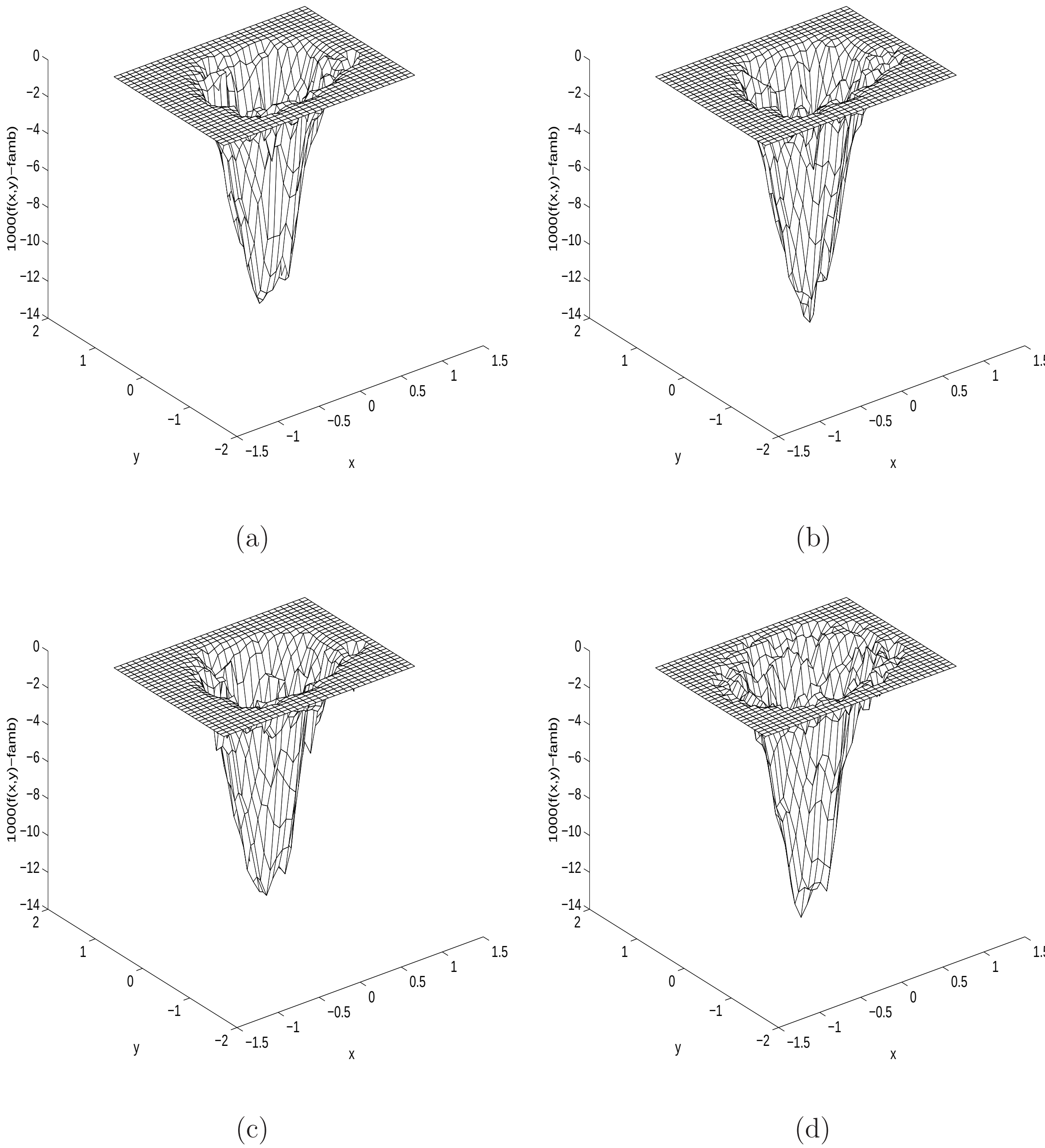

Fig. 8. Reconstructed surface mesh pro les of the phantom $P2$ obtained for the data set $P2D2$ after the second iteration by (a) the Haar MR-EKF, (b) the Db-4 MR-EKF, (c) the SR-EKF, and, (d) the ACP algorithm.

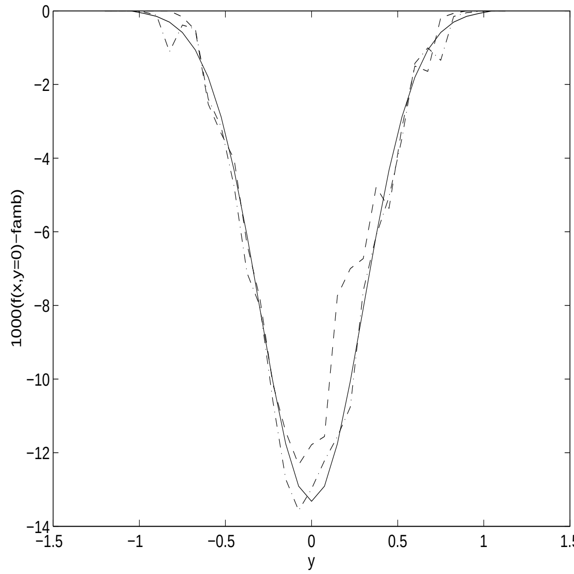

(a)

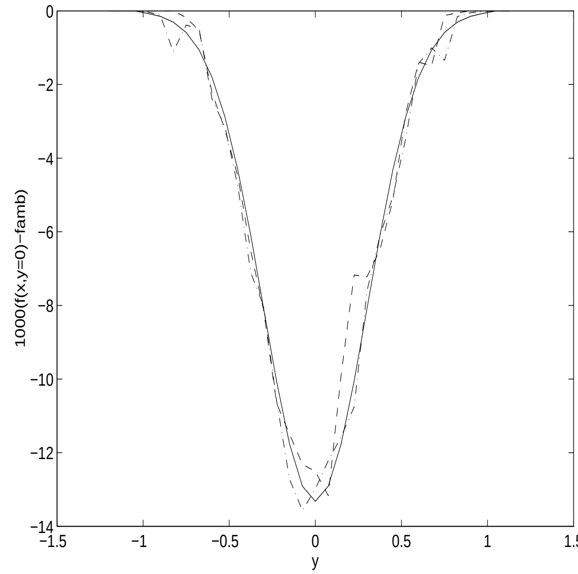

(b)

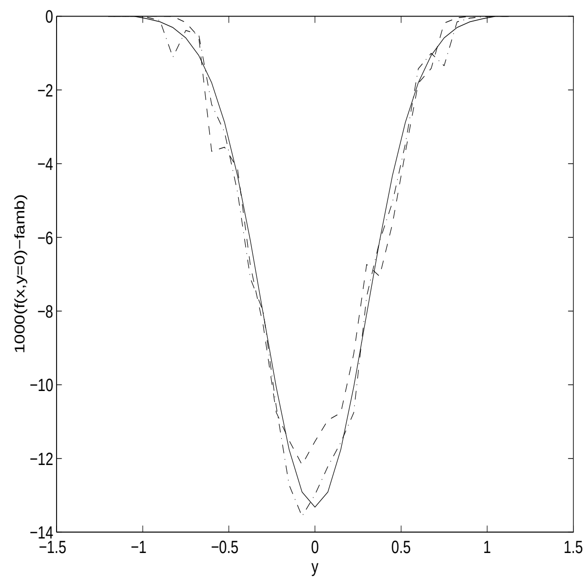

(c)

Fig. 9. Reconstructed profiles of the $x = 0$ plane of phantom $P2$ obtained from the EKFs(dashed curves), as compared to ACP (dot-dash curve) algorithm and the actual profile (solid line) for the data set $P2D2$ after the second iteration by (a) the Haar MR-EKF, (b) the Db-4 MR-EKF, and, (c) the SR-EKF algorithm.

are adaptively estimated. The initialization of the biases and covariances corresponding to the state and measurement noise is discussed. An EKF is then applied to the wavelet transformed state variable model to yield a wavelet based multiresolution EKF (MR-EKF) solution approach.

The SR-EKF and two versions of the MR-EKF (with respectively Haar and Daubechies-4 wavelets) are validated by numerical studies of reconstructions of two synthetic RIDs from OPD data sets of various noise levels. The EKF results compare well with those obtained from an e cient typically used variant of the algebraic reconstruction technique, the ACP method, thus establishing the capability of the adaptive estimation based EKF for ORT. To the best of our knowledge, this work contains unique reconstruction studies in ORT encompassing the single/multi-resolution EKF, and the use of adaptive estimation of the EKF s noise covariances in nonlinear tomography.

The results obtained in this work thus provide a good understanding and validation of the use of adaptive EKFs in the ORT problem and provide the essential prerequisite for interesting issues that need to be addressed in future works, including (a) the development of schemes for time-varying RIDs, and, (b) the development of adaptive re nement schemes that add/delete detail coe cients in the wavelet domain.

Appendix A:Orthonormal discrete wavelet transform

Consider a vector $\mathbf{f}$, of length $N = 2^{\ p}$, for some positive integer p. Introduce the function $f(x)$, de ned as

$$f(x) = \sum_{k=0}^{N\ \ 1} f_k \ \ {}_{p\,k}(x) \tag{23}$$

where ${}_{j\,k}(x) = 2^{\ j\ 2}\ \ (2^{\ j}x \ \ \ k)$,

where ${}_{0\,0}(x) = \ \ (x)$, is the scaling function, which in our present work is taken to be of compact support. We denote the corresponding mother wavelet of compact support as $\ \ (x)$.

The discrete wavelet transform (DWT) [31], [51], [52], of the signal $\mathbf{f}$, is constituted by the coe cients of the expansion of $f(x)$ in (a) the approximate subspace spanned by the basis set $\ \ {}_{p+j\,k}(x)\ k \ \ \mathbf{Z}$, and (b) the detail subspaces spanned by basis set $\ \ {}_{p+i\,k}(x)\ i = 1\ 2 \ \ \ \ j; k \ \ \mathbf{Z}$, where, ${}_{j\,k}(x) = 2^{\ j\ 2}\ \ (2^{\ j}x \ \ \ k)$.

De ne,for xed M, and given N, the lters, $H_N^M\ G_N^M : l^2 \ \ \ l^2$ as

$$(H_N^M\mathbf{f})_l = \sum_{k\ \mathbf{Z}} h_{k\ \ 2l} f_k \tag{24}$$

$$(G_N^M\mathbf{f})_l = \sum_{k\ \mathbf{Z}} g_{k\ \ 2l} f_k \tag{25}$$

where $\ \ (x) = \ \ \overline{2}\ \ {}_{k=0}^{2M\ \ 1} h_k\ \ (2x \ \ \ k)$

where only $h_0\ h_1 \ \ \ \ h_{2M\ \ 1} \ \ \ \ \mathbf{R}$ have nonzero values, and $\ \ (x) = \ \ \overline{2}\ \ {}_{k=0}^{2M\ \ 1} g_k\ \ (2x \ \ \ k)$, with $g_k = (\ \ 1)^k h_{2M\ \ 1\ \ k}$. Periodising the matrix forms of the above operators, to avoid edge e ects for $M > 1$, we get the $N\ 2 \ \ \ N$ matrix representation of the above operators, $\mathcal{H}_N$ and $\mathcal{G}_N$ (where the M in the superscript has been left out for ease of notation), as

$$
\mathcal{H}_N = \begin{array}{cccccc}
h_0 & & h_{2M \ \ 1} & & & \\
 & & & h_0 & h_{2M \ \ 1} & \\
h_{2M \ \ 2} \ \ h_{2M \ \ 1} & & & & h_0 & h_{2M \ \ 3} \\
h_2 & h_{2M \ \ 1} & & & h_0 & h_1
\end{array} \tag{26}
$$

$\mathcal{G}_N$ is of the same form as $\mathcal{H}_N$, with the g_k replacing the corresponding h_k. Operating these matrices on $\mathbf{f}$ has the same result as operating the originally de ned lters on a periodized version of $\mathbf{f}$. The N 2 length vectors $\mathcal{A}_N\mathbf{f}$ and $\mathcal{G}_N\mathbf{f}$ are called the approximate(low-pass ltered version) and detail (high-pass ltered version) components respectively, of the DWT of the signal $\mathbf{f}$. Hence the DWT, $\mathbf{f}$, of the signal $\mathbf{f}$ at level j is given by [52]

$$
\mathbf{f}^{(j)} = \mathbf{W}_1^{(j)}\mathbf{f} = \begin{array}{c}
\mathcal{H}_{N \ 2^j \ \ 1} \\
\vdots \\
\mathcal{G}_{N \ 2^2}\mathcal{H}_{N \ 2} \\
\mathcal{G}_{N \ 2}\mathcal{H}_N \\
\mathcal{G}_N
\end{array} \tag{27}
$$

where the suitably formed wavelet transform matrix, $\mathbf{W}_1^{(j)}$ is an orthonormal matrix, the subscript in $\mathbf{W}$ denoting the dimensionality of the transformed signal.

The decomposition scheme of a two-dimensional $N \times N$ image, $\mathbf{F}$, based on $2D$ separable multiresolution wavelet bases is a straightforward extension of the $1D$ case.

The $2D$ discrete wavelet transform(DWT) [31], [51], $\mathbf{F}^{(1)}$ of the image $\mathbf{F}$, at level $j = 1$, is given by,

$$\mathbf{F}^{(1)} = \mathbf{W}_1^{(1)} \mathbf{F} \mathbf{W}_1^{(1)} \tag{28}$$

The image $\mathbf{F}^{(1)}$ consists of one approximate sub-image, $\mathcal{A}^{(1)}$, and three detail sub-images, $\mathcal{D}^{(1)}_i$, $i = 1, 2, 3$, which are given by, $\mathcal{A}^{(1)} = \mathcal{H}_N \mathbf{F} \mathcal{H}_N$, $\mathcal{D}_1^{(1)} = \mathcal{H}_N \mathbf{F} \mathcal{G}_N$, $\mathcal{D}_2^{(1)} = \mathcal{G}_N \mathbf{F} \mathcal{H}_N$, and $\mathcal{D}_3^{(1)} = \mathcal{G}_N \mathbf{F} \mathcal{G}_N$.

Defining $\mathbf{f}$ as the vector obtained by lexicographically ordering the image $\mathbf{F}$, we obtain the wavelet transformed vector $\mathbf{f}$ as,

$$\mathbf{f}^{(j)} = \mathbf{W}_2^{(1)} \mathbf{f} \tag{29}$$

where $\mathbf{W}_2^{(1)} = \mathbf{W}_1^{(1)} \otimes \mathbf{W}_1^{(1)}$, $\otimes$ denoting the Kronecker product.

Appendix B: List of acronyms

ACP : Average correction per projection, ART : Algebraic reconstruction technique, DWT : Discrete wavelet transform, EECM : Estimation error covariance matrix, EKF : Extended Kalman filter, MR-EKF : Multiresolution EKF, OPD : Optical path-length difference, ORT : Optical refraction tomography, RID : Refractive index distribution, SART: Simultaneous algebraic reconstruction technique, SR-EKF : Single resolution EKF, SV : State variable.

References

1. C.M. Vest, Tomography for properties of materials that bend rays: a tutorial , Appl. Opt., **24**, 4089 (1985).
2. G.W. Faris and R.L. Byer, Beam de ection optical tomography of a ame , Opt. Lett., **12**, 155 157 (1987).
3. G.W. Faris and R.L. Byer, Three dimensional beam de ection optical tomography of a supersonic jet , App. Opt., **27**, 5202 5212 (1988).
4. Y. Song, B. Zhang and A. He, Algebraic iterative algorithm for de ection tomography and its application to density ow elds in a hypersonic wind tunnel , Appl. Opt., **45**(31), 8092 8101 (2006).
5. I.H.Lira, *Correcting for refraction e ects in holographic interferometry and tomography of transparent objects* (PhD Thesis, University of Michigan, Ann Arbor,1987).
6. S.Bahl and J.A.Liburdy , Three dimensional image reconstruction using interferometric data from a limited eld of view with noise , App. Opt., **30**, 4218 4226(1991).
7. B.H. Timmerman, D.W. Watt and P.J. Bryanston-Cross, Quantitative visualization of high speed 3D turbulent ow structures using holographic interferometric tomography , Opt. Laser Technol., **31**, 53 65(1999).
8. Naren Naik, *Studies on the development of models and reconstruction algorithms*

for optical tomography, (Ph.D. thesis, Department of Instrumentation, Indian Institute of Science, Bangalore, 2000).

9. G. Keshava Datta, R.M. Vasu, Non-interferometric methods of phase estimation for application in optical tomography , J. Mod. Opt., **46**, 1377 1388(1999).

10. A. Barty, K.A. Nugent, A.Roberts and D. Paganin, Quantitative phase microscopy , Opt. Commun., **175**, 329 336(2000).

11. H. Thayyullathil, R. Langoju, R. Padmaram, R.M. Vasu, R. Kanjirodan and L.M. Patnaik, Three-dimensional optical tomographic imaging of supersonic jets through inversion of phase data obtained through inversion of phase data obtained through the transport of intensity equation , Appl. Opt., **43**,4133 4141(2004).

12. R.E Pierson, D.F. Olson and E.Y. Chen and L. Mc Mackin, Comparison of reconstruction algorithm performance for optical phase tomography of a heated air ow , Opt. Eng., **39**, 838 846 (2000).

13. H. Thayyullathil, R.M. Vasu and R. Kanjirodan, Quantitative ow visualisation in supersonic jets through tomographic inversion of wavefronts estimated through shadow casting , Appl. Opt., **45**, 5010 5019 (2006).

14. A.H.Andersen and A.C.Kak, Simultaneous algebraic reconstruction technique (SART): a superior implementation of the ART algorithm , *Ultrasonic Imaging*, **6**, 81 94(1984).

15. F.Denis, O.Basset and G.Gimenez, Ultrasonic transmission tomography in re-

fracting media : Reduction of refraction artifacts by curved ray techniques ,
IEEE Trans. Med. Imag., **14**, 173 188 (1995).

16. R.J.Lytle and K.A.Dines, Iterative ray tracing between boreholes for underground image reconstructions , IEEE Trans Geosc. Rem. Sens., **GE-18**, 234 240 (1980).
17. James G.Berryman, Fermat s principle and nonlinear traveltime tomography ,Phy. Rev. Letts, **62**, 2953 2956 (1989).
18. Shin-yee Lu and James G.Berryman, Inverse scattering, seismic traveltime tomography, and neural networks Intl. Jl. Imag. Sc. Tech., **2**, 112 118(1990).
19. I.H.Lira and C.M.Vest, Refraction correction in holographic interferometry and tomography of transparent objects , App. Opt., **26**, 3919 3928(1987).
20. S.Cha and C.M.Vest, Tomographic reconstruction of strongly refracting elds and its application to interferometric measurement of boundary layers , App. Opt., **20**, 2787 2794 (1981).
21. S.J.Norton and J.M.Linzer, Correcting for ray refraction in velocity and attenuation tomography : A perturbation approach , Ultrasonic Imaging, **4**, 201 233 (1981).
22. Ray Snyder and Lambertus Hesselink, High speed optical tomography for ow visualisation , App. Opt., **24**, 4046 4051, (1985).
23. M. J. Eppstein and D.E. Dougherty, Optimal 3-D traveltime tomography , Geo-

physics, **63**(3), 1053 1061, (1998).

24. M. J. Eppstein, D.E. Dougherty, T.L. Troy and E. M. Sevick-Muraca, Biomedical optical tomography using dynamic parametrization and Bayesian conditioning on photon migration measurements , Appl. Opt., **38**(10), 2138 2150, (1999).

25. Naren Naik and R.M Vasu , An extended Kalman lter based reconstruction approach to curved ray optical tomography , Proc. SPIE, **3729**, 153 157 (1999).

26. Naren Naik and R.M Vasu , A wavelet based multiresolution extended Kalman lter approach to the reconstruction problem of curved ray optical tomography , *High-Speed Imaging and Sequence Analysis*, Eds. Alan M. Frank, James S Walton, 156 165, Proc. of SPIE Vol. **3642**(1999).

27. V. Kolehmainen, S. Prince, S.R. Arridge and J.P. Kaipio, State estimation approach to the nonstationary optical tomography problem , J. Opt. Soc. Am. A, **20**, 876 889 (2003).

28. A-P Tossavainen, M. Vauhkonen, V. Kolehmainen, A three-dimensional shape estimation approach for tracking of phase interfaces in sedimentation processes using electrical impedance tomography , Meas. Sci. Technol.,**18**, 1413 1424 (2007).

29. Seppanen, M. Vaukhonen, E.Somersalo and J.P. Kaipio, State space models in process tomography approximation of state noise covariance, Inverse Problems in Engineering, **9**, 561 585 (2001).

30. B.Banerjee, D. Roy and R. M. Vasu, A pseudo-dynamic sub-optimal lter for

elastography under static loading and measurements , Phys. Med. Biol., **54**, 285-305 (2009).

31. Ingrid Daubechies, *Ten lectures on wavelets*, (SIAM, Pennsylvania, 1992).
32. T.M.Chin and A.J.Mariano, Wavelet based compression of covariances in Kalman ltering of geophysical ows , Proc.SPIE, **2242**, 842 850, (1994).
33. T.M.Chin and A.J.Mariano, Kalman ltering of large scale geophysical ows by approximations based on Markov random elds and wavelets , Proc.IEEE Intl.Conf.Acoust.Sp.Sig.Proc., **5**, 2785 2788 (1995).
34. G.Beylkin, R.R.Coifman, and V.Rokhlin, Fast wavelet transforms and numerical algorithms , Comm. Pure and App l. Math., **44**, 141 183 (1991).
35. A.H.Andersen, Ray linking for computed tomography by rebinning of projection data , J.Acoust.Soc.Am, **81**, 1190 1192 (1987).
36. P. Maybeck, *Stochastic models, estimation and control*, (Academic Press, 1982).
37. A. K. Sarkar, *New prespectives in state and parameter estimation of ight vehicles for o -line and real time applications*, (Ph.D. Thesis, Department of Aerospace Engineering, Indian Institute of Science, Bangalore, November 2004).
38. E.L.Miller, L.Nicolaides and A.Mandelis, Nonlinear inverse scattering methods for thermal wave slice tomography : A wavelet domain approach , J. Opt. Soc. Am. A, **15**, 1545 1556 (1998).
39. A.H.Andersen and A.C.Kak, Digital ray tracing in two dimensional refractive

elds , J. Acoust. Soc. Am **72**, 1593 1606 (1982).

40. A.H.Jazwinski, *Stochastic processes and ltering theory*, (Academic Press, New York, 1970).

41. J.M.Mendel, *Lessons in digital estimation theory* , (Prentice Hall, Englewood Cli s, New Jersey, 1987).

42. K.A.Myers and B.D.Tapley, Adaptive sequential estimation with unknown noise statistics , IEEE Trans. Aut. Cont.,**AC-21**, 520 523 (1976).

43. R.L.Kirlin and A.Moghaddamjoo, Robust adaptive Kalman ltering for systems with unknown step inputs and non-Gaussian measurement errors , IEEE Trans Acoust.Sp and Sig.Proc., **ASSP-34**, 252 263 (1986).

44. L.Blanc-Feraud, P.Charbonnier, P.Lobel and M.Barlaud, A fast tomographic reconstruction algorithm in the 2D-wavelet transform domain , Proc.IEEE Intl.Conf.Acoust.Sp.Sig.Proc., **5**, 305 308 (1994).

45. I. Daubechies, M. Defrise and C. de Mol, An iterative thresholding algorithm for linear inverse problems with a sparsity constraint , Commun. Pure Appl. Math., 57(11), 1413 1457 (2004).

46. W.Zhu, Y.Deng, Y.Yao, and R.L.Barbour A wavelet based multiresolution regularised least squares reconstruction approach to optical tomography , IEEE Trans. Med. Imag.,**16**, 210 217 (1997).

47. P.Charbonnier, L.Blanc-Feraud, G.Aubert, and M.Barlund, Deterministic edge

preserving regularization in computed imaging , IEEE Trans. Image Proc., **6**, 298 311 (1997).

48. A.C.Kak and M.Slaney, *Principles of computerised tomographic imaging*, (IEEE Press, New York, 1988).

49. G.J.Bierman, *Factorisation methods for discrete sequential estimation* (Academic Press, 1977).

50. D.D.Verhoeven, MART type CT algorithms for the reconstruction of multi-directional interferometric data , *Laser Interferometry IV : Computer Aided Interferometry*, 376-387, Proc. of SPIE, **1553** (1991).

51. T. H. Koornwinder, *Wavelets:An elementary treatment of theory and applications*, (World Scienti c, 1993).

52. B.Lin, B. Nguyen and E. T.Olsen, Orthogonal wavelets and signal processing , *Signal processing methods for audio, images and telecommunication*, Eds. Peter M.Clarkson and Henry Stark, 1-69 (Academic Press, London, 1995).